Engineering Structures 195 (2019) 551–558

Contents lists available at ScienceDirect

Engineering Structures

journal homepage: www.elsevier.com/locate/engstruct

Testing and modeling of dowel action for a post-installed anchor subjected to combined shear force and tensile force

Yuya Takase

College of Environmental Technology, Muroran Institute of Technology, Japan

ARTICLE INFO

Keywords:
Post-installed anchor
Seismic retrofit
Dowel action
Combined stress
Mechanical behavior
Concrete structures
Supporting stress

ABSTRACT

In seismically active regions, the resistance of buildings against earthquakes must be improved. Post-installed anchors are generally used to connect retrofitting members to existing concrete members of a structure. However, research on the mechanical behavior of post-installed anchors subjected to combined shear and tensile stress is insufficient. Therefore, in this study, loading tests were conducted on anchor bolts by applying cyclic shear loading and constant tensile forces. Additionally, a mechanical model was constructed to evaluate the experimental results. In this model, the shear force was equal to the sum of the bending resistant force at the plastic hinge, the supporting stress of the concrete, and the shear component of the tensile stress of the anchor bolt. The results demonstrate that, with increasing tensile force, the shear force decreases and the joint separation increases. In addition, the proposed model was shown to reasonably replicate the shear load and slip relationship determined from experimentation results.

1. Introduction

In seismically active regions, seismic retrofits are often used to improve the resistance of buildings against earthquakes. Commonly, retrofitting is achieved by connecting strengthening members to existing members of a structure by using post-installed anchors. During an earthquake, these anchors distribute the shear stress by dowel action and catenary action in the reinforced concrete structures [1], therefore post-installed anchors are very vital elements.

Although the retrofitting members are typically internally connected within an existing structure, the method of externally connecting them is gaining popularity. Fig. 1 shows an image of an external seismic retrofit. The main advantage of an externally connected seismic retrofit, as opposed to its internally connected counterpart, is that the construction will not obstruct the internal functions of the building. At the joints of such structures, a tensile force is caused by bending moments acting between the existing and expanding frames. Therefore, the joints of the structures with externally connected retrofits are subjected to both shear and tensile forces. However, it is thought that the vertical loading slightly affects the shear strengths of the post-installed anchors, but this paper focuses on the shear behaviors as an early step in the investigation of the anchors.

Distribution of the shear stress of reinforced bars in concrete occurs by dowel action. Since Friberg's study on dowel action in the 1930s [2], many researchers have studied this topic [1,3–12], with most studies primarily focusing on the linear elastic models of one-sided dowel action. Recently, a nonlinear dowel model was proposed by Sorensen [1], and a dowel model was implemented in finite element analysis by He [11]. Although Soltani and Maekawa proposed the model under coupled cyclic shear and pull out tension for a reinforcing bar, in this model, catenary action was not taken into account [12].

As previously mentioned, because externally connected post-installed anchors are subjected to a combined shear/tensile force, it is important to understand the mechanical behavior of post-installed anchors. However, despite its significance, only a few studies have focused on the mechanical behavior of post-installed anchors. Shirai conducted an experimental study on post-installed anchors subjected to transverse diagonal loading [13]. However, the tensile and shear forces were considered, the findings of that study do not adequately describe the mechanical behavior.

The author previously conducted several fundamental tests related to the dowel action of post-installed anchors subjected to pure shear force, and tried to construct a fundamental model [14]. Building on the previous study, in the current study, shear loading tests were conducted on post-installed anchors subjected to constant tensile force as based on the optimized design of dowel action in the external connection of the anchors. Moreover, a mechanical model was proposed in this study to estimate the relationship between shear load and slip under a combined force. In this model, the both dowel action and catenary action were taken into account.

E-mail address: y.takase@mmm.muroran-it.ac.jp.

https://doi.org/10.1016/j.engstruct.2019.05.086
Received 1 April 2018; Received in revised form 16 March 2019; Accepted 27 May 2019
Available online 21 June 2019

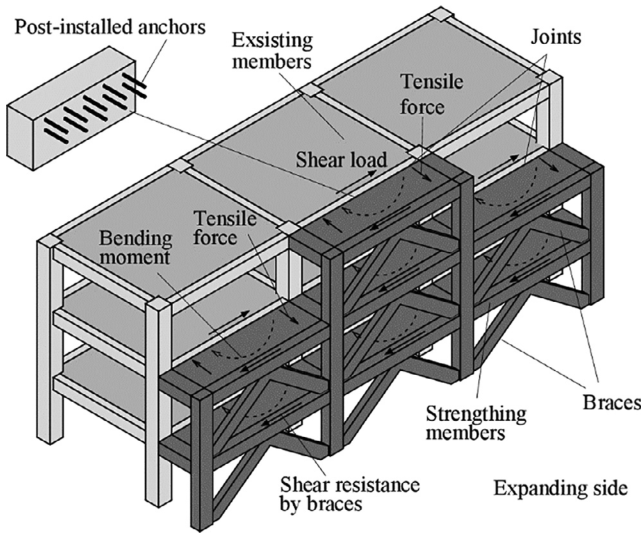

Fig. 1. Diagram of external seismic retrofit.

2. Experimental program

Fig. 2 shows the mechanism of shear-stress transfer in a post-installed anchor subjected to combined force. In this section, the experimental program is described.

2.1. Test parameters

Table 1 shows the individual characteristics of 13 specimens tested in this paper. The experimental parameters include a diameter ϕ, a concrete compressive strength f_c, and tensile stress on the anchor f_N. The diameters of the deformed bars used as anchor bolts are 13 mm, 16 mm, and 19 mm. f_c is set as 10, 20, and 30 N/mm^2, as is common in older buildings, and f_N is set as approximately 0, 0.33f_y, and 0.66f_y N/mm^2, where f_y is the yield strength of the anchor bolt. Because of a lack of specimens, those with an f_c of 10 and 30 N/mm^2 were only tested at $f_N = 0$ and $0.56f_y$ N/mm^2. Subsequently, the tensile stress ratio $r_N = f_N/f_y$ is used as the index instead of f_N.

The specimens were named according to their specifications; the number that follows the first letter D indicates the diameter ϕ, followed by the parameter values for r_N and f_c.

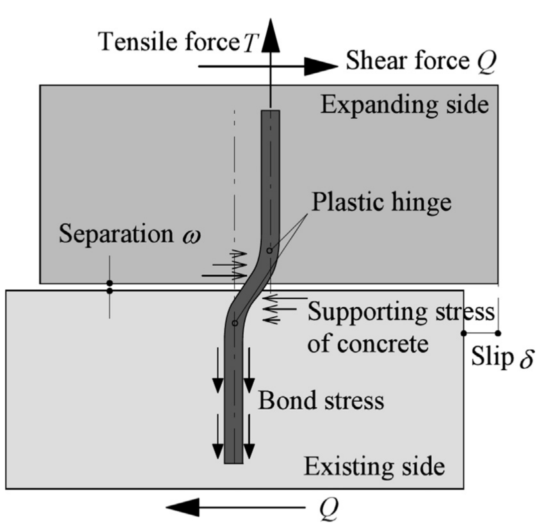

Fig. 2. Mechanism of shear stress transfer of post-installed anchor under combined force.

Table 1
Experimental test parameters.

Specimen no.	ϕ (mm)	r_N	Fc (N/mm^2)	Le (mm)	Grouting mortal
D13-T000-20	13	0	20	10ϕ	Property-1
D13-T033-20	13	0.33	20	10ϕ	Property-1
D13-T066-20	13	0.66	20	10ϕ	Property-1
D16-T000-10	16	0	10	10ϕ	Property-2
D16-T056-10	16	0.56	10	10ϕ	Property-2
D16-T000-20	16	0	20	10ϕ	Property-1
D16-T033-20	16	0.33	20	10ϕ	Property-1
D16-T066-20	16	0.66	20	10ϕ	Property-1
D16-T000-30	16	0	30	10ϕ	Property-2
D16-T056-30	16	0.56	30	10ϕ	Property-2
D19-T000-20	19	0	20	10ϕ	Property-1
D19-T033-20	19	0.33	20	10ϕ	Property-3
D19-T066-20	19	0.66	20	10ϕ	Property-1

ϕ: Diameter of anchor-bolt, r_N: Tensile force ratio, F_c: Designed concrete compressive strength.

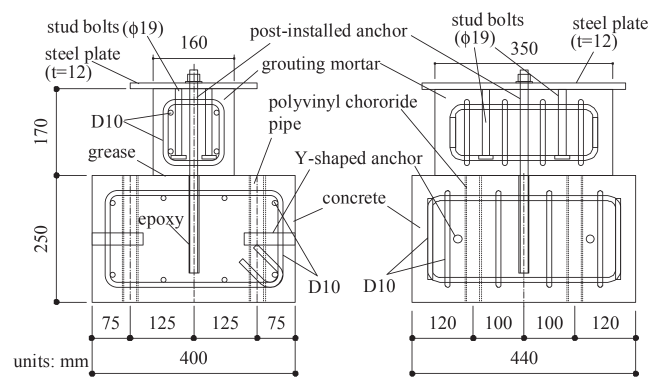

Fig. 3. Details of specimen.

Table 2
Concrete and grouting mortal properties.

Specimen no.	f_c (N/mm^2)	E_c (N/mm^2)	f_t (N/mm^2)
F_c = 10 N/mm^2	12.5	18.1	1.43
F_c = 20 N/mm^2	20.1	23.8	1.93
F_c = 30 N/mm^2	30.5	25.9	1.93
Grouting mortal-1	59.1	23.6	3.30
Grouting mortal-2	70.7	24.6	3.00
Grouting mortal-3	72.6	23.4	3.28

f_c: Concrete compressive strength, E_c: Young's modulus, f_t: Concrete split strength.

Table 3
Anchor-bolt properties.

ϕ (mm)	f_y (N/mm^2)	f_u (N/mm^2)	E_s (kN/mm^2)	δ (%)
13	375	582	193	26
16	396	582	194	24
19	402	600	189	23

f_y: Yield strength, f_u: Ultimate strength, E_s: Young's modulus, δ: Elongation after fracture.

2.2. Test specimens

Fig. 3 shows details of the specimens. Table 2 outlines the material properties of the concrete and the mortar, and Table 3 shows those of the anchor bolts.

The specimens used to model the existing members are 440 mm × 400 mm × 250 mm reinforced concrete blocks, and those used to model the supporting members are

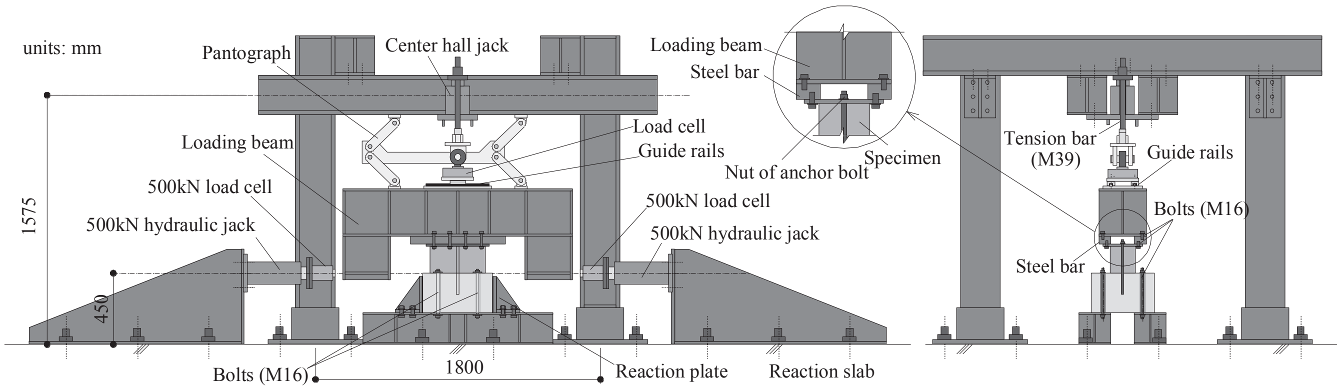

Fig. 4. Loading setup.

350 mm × 170 mm × 160 mm grouting mortar blocks with reinforcing bars of ϕ = 10 mm. Post-installed anchors were adhered to the concrete blocks, and the grouting mortar blocks were constructed around them. Normal-weight concrete was used to cast the specimens.

The joining surfaces between the concrete and grouting mortar were greased in order to minimize the effects of friction. To connect the post-installed anchors, a rotary hammer was used for drilling, and injectable epoxy adhesives were applied for anchoring.

2.3. Loading and measurement method

Fig. 4 shows the loading setup, and the measurement method is illustrated in Fig. 5. The test specimens were subjected to a cyclic shear force and a constant tensile force from the loading equipment shown in Fig. 4. The two hydraulic jacks and one center-hall jack were used to apply shear loading and tensile loading, respectively, and the test specimens were fixed to the reaction beam and loading beam. The loading beam was attached to the loading frame by using a pantograph, thereby enabling horizontal displacement during shear loading.

Note that the slip δ and the separation ω are the average values of the relative horizontal displacement and the vertical displacement, respectively. In addition, the loading cycle is illustrated in Fig. 6.

3. Experimental results

3.1. Relationship between tensile force ratio and shear force ratio

Ordinarily, when the combined stresses of steel are calculated, the von Mises stress is often applied. Moreover, this stress is only applied under the condition of simple shear and normal stress. However, because the stress field of the tests performed in this study was significantly more complex, a strength formula, such as that given as Eq.

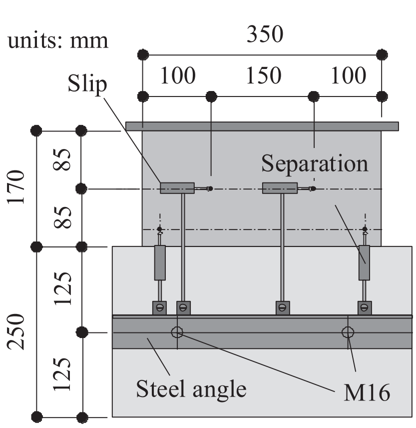

Fig. 5. Measurement method.

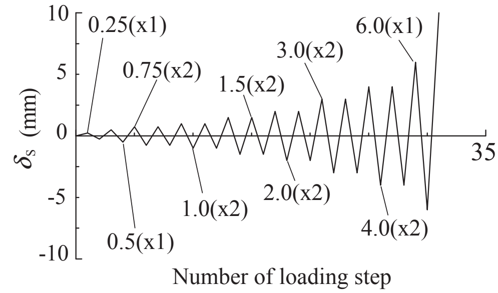

Fig. 6. Loading cycle.

(1), that is generally applied to structural designs subjected to combined force was used.

$$(T/T_a)^\alpha + (Q/Q_a)^\alpha = 1 \tag{1}$$

where T_a and Q_a are the specific tensile strength and shear strength of an anchor bolt, respectively, and T and Q are the tensile force and shear force, respectively, that are allowed under a combined stress. α is an experimental coefficient that generally takes a value between 1 and 2.

T_a is expressed as follows:

$$T_a = a_s \times f_y \tag{2}$$

where a_s is the cross-sectional area of an anchor bolt.

A shear strength formula for an anchor bolt can be used to determine Q_a. However, these formulas can considerably differ from test results. Therefore, the shear force Q obtained from testing with $r_N = 0$ is used instead of Q_a to solve Eq. (1). Using this value, the results of the specimens with $r_N = 0$ can be directly compared to those of the specimens under tensile stress.

Fig. 7 shows the relationship between T/T_a and Q/Q_a that was obtained by way of loading testing for δ= 0.25, 0.75, 1.0, 2.0, 3.0, and 4.0 mm. The test results revealed α ranged from 0.75 to 1.5. Specifically, a smaller slip, i.e., δ = 0.25–0.75, yielded an α value ranging from 0.5 to 1.0, whereas, a slip larger than δ = 1.0 yielded an α range of 1.0–1.5.

3.2. Relationship between separation and slip

Fig. 8 shows the relationship between separation ω and slip δ. It is evident that ω increased with increasing tensile force. As an example, in the case of $r_N = 0$, ω remained at a value of less than 1 mm, even for δ = 6 mm. However, for r_N = 0.33 and r_N = 0.56–0.66, ω was observed to exceed 1 mm before the slip δ reached a value of 2 mm. Furthermore, because the average separation ω of the second step was larger than that of the first step, it is essential that the number of loading cycles be considered. Additionally, the remaining separations of specimens with r_N = 0.33 and r_N = 0.56–0.66 were found to be larger than those with

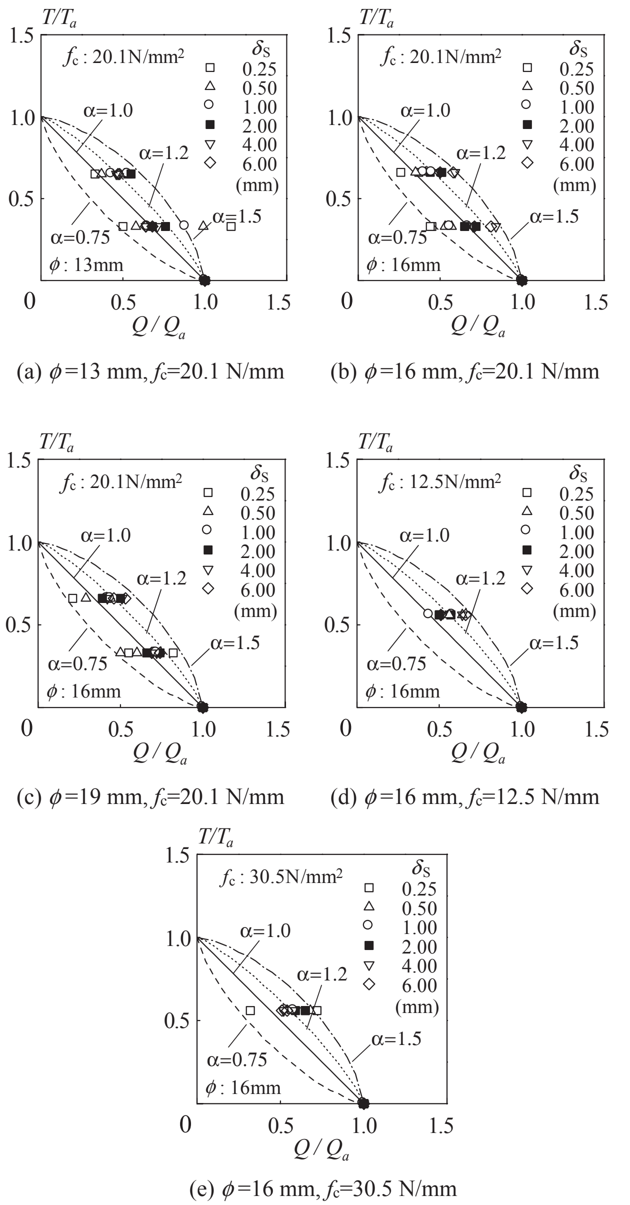

(a) ϕ=13 mm, f_c=20.1 N/mm (b) ϕ=16 mm, f_c=20.1 N/mm

(c) ϕ=19 mm, f_c=20.1 N/mm (d) ϕ=16 mm, f_c=12.5 N/mm

(e) ϕ=16 mm, f_c=30.5 N/mm

Fig. 7. Shear stress ratio – tensile stress ratio relations.

$r_N = 0$. The resulting separation tendency of specimens with $\phi = 16$ mm and 19 mm was found to be similar to that of a specimen with $\phi = 13$ mm. It should also be noted that the amount of separation was also comparable to the diameter of the anchor bolts, and that the influence of the concrete compressive strength on the amount of separation was small.

4. Proposed model

To realize the aim of this study, which was to construct a mechanical model of an adhesive post-installed anchor subjected to a combined force, a mechanical model that considers the following two failure modes of post-installed anchors is proposed: (i) the yielding of the anchor bolt and (ii) the supporting failure of concrete. This chapter describes the proposed model in detail.

4.1. Equilibrium of shear force

Fig. 9 illustrates how dowel action was modeled for a post-installed anchor. When the displacement is small, it is possible to apply the elastic beam theory to a post-installed anchor. However, because elastic beam theory cannot be extended to the case in which the anchor bolt or concrete is within its plastic range, the model shown in Fig. 9 has been proposed to better describe the behavior in a nonlinear zone.

To construct the proposed model, the plastic behavior of the anchor bolt at the bending point (the hinge) was initially calculated. Because it was assumed that the anchor bolt deforms in a linear manner about the plastic hinge, the supporting stress must act on the concrete. Additionally, the modeled anchor bolt tended to elongate between the concrete surface and plastic hinge, thereby making the anchor bolt subject to tensile stress with a significant shear component. As was mentioned above, when $r_N = 0$, the shear force q_0 equates to the sum of (i) the bending moment of the plastic hinge q_S, (ii) the supporting stress of the concrete q_B, and (iii) the shear component of the tensile stress of the anchor bolt q_T^s by catenary action.

$$q_0 = q_S + q_B + q_T^s \tag{3}$$

In addition, the shear force$q$ when the anchor bolt is subjected to tensile force is expressed as is described in the following equation, which is derived from Eq. (1):

$$q = \sqrt[\alpha]{1 - (T/T_a)^\alpha} \times q_0 \tag{4}$$

Here, α is set to 1 from the test results.

4.2. Depth of plastic hinge

As was mentioned in the Section 4.1, the depth of plastic hinge L_h is needed to calculate, because L_h influences the three components of the shear force. According to the elastic beam theory, the depth of the largest moment L_M can be calculated as follows:

$$L_M = \frac{\pi}{4}\sqrt[4]{\frac{4 \times E_s \times I_z}{\kappa \times \phi}} \tag{5}$$

where κ is the supporting stiffness of the concrete and I_z is the second section moment of the anchor bolt.

However, when concrete is in its plastic range, κ is relatively small. This means that, within this range, the small κ causes L_M to be relatively larger. Therefore, the following equation, which takes three-halves of L_M, is implemented as L_h in the proposed model.

$$L_h = \frac{3\pi}{8}\sqrt[4]{\frac{4 \times E_s \times I_z}{\kappa \times \phi}} \tag{6}$$

Then, κ is obtained by solving the equation below, which was derived in a previous study [12].

$$\kappa = 150 f_c^{0.85}/\phi \tag{7}$$

where f_c is the compressive strength applied on the concrete (N/mm^2).

4.3. Supporting stress of concrete

The concrete strain around an anchor bolt is influenced by the deformation of the anchor bolt. Assuming that the anchor bolt linearly deforms about the plastic hinge, the displacement $\delta(x)$ is described as follows.

$$\delta(x) = \delta(0) - \frac{\delta(0)}{L_h}x \quad \text{for} \quad 0 \le x \le L_h \tag{8}$$

$$\delta(x) = 0 \quad \text{for} \quad L_h < x \tag{9}$$

where x is the depth from the joint surface.

Although concrete strain is considered to be the highest near the anchor bolt, and thus decreasing with increased distance from the anchor bolt, it is difficult to provide evidence of this phenomenon. In this study, the concrete strain is described as the average strain.

$$\varepsilon_b(x) = \delta(x)/L_{\varepsilon b} \tag{10}$$

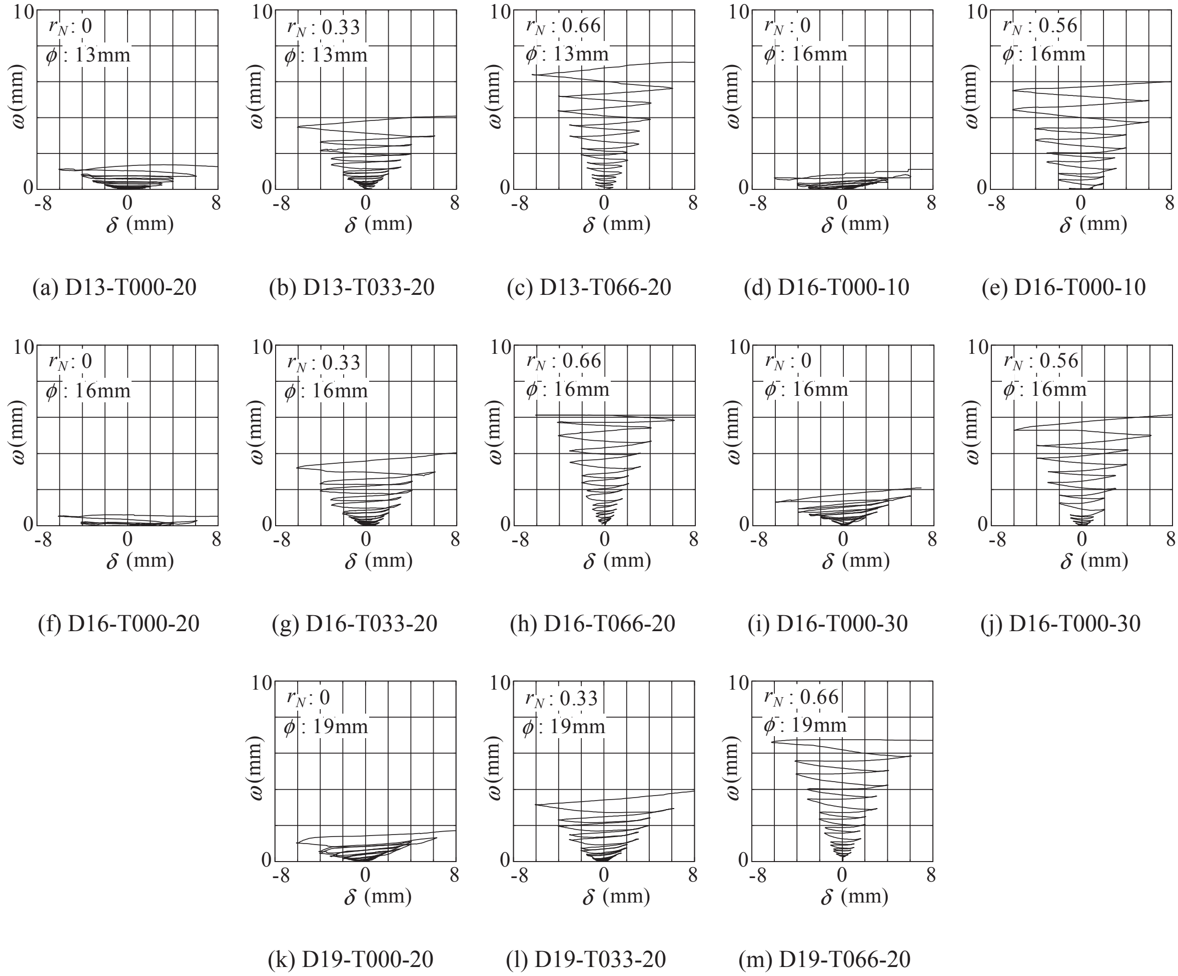

Fig. 8. Joint opening – slip relations curves.

where $L_{\varepsilon b}$ is the effective length used to calculate the concrete strain; $L_{\varepsilon b}$ was set as 5ϕ.

The supporting force of the concrete q_B was calculated by multiplying the circumference of the semicircle of the anchor bolt by the integral of the supporting stress from $x = 0$ to $x = L_h$.

$$q_B = \frac{\pi\phi}{2}\int_0^{L_h} f_b(x)dx \tag{11}$$

4.4. Tensile stress of anchor bolt

When the anchor bolt deforms about the plastic hinge, it is stretched between the hinge point and the concrete surface by catenary action. The increase in length ΔL_{br} is expressed as follows:

$$\Delta L_{br} = \sqrt{\delta_a^2 + L_h^2} - L_h \tag{12}$$

$$\Delta\varepsilon_{br} = \Delta L_{br}/L_h \tag{13}$$

As is given in Eq. (13), ΔL_{br} is used to determine the increasing

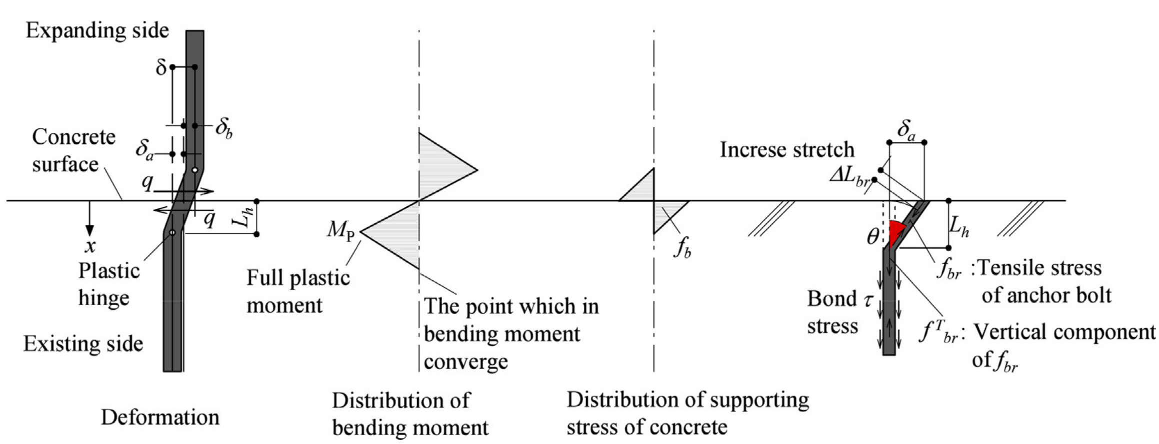

Fig. 9. Image of proposed model.

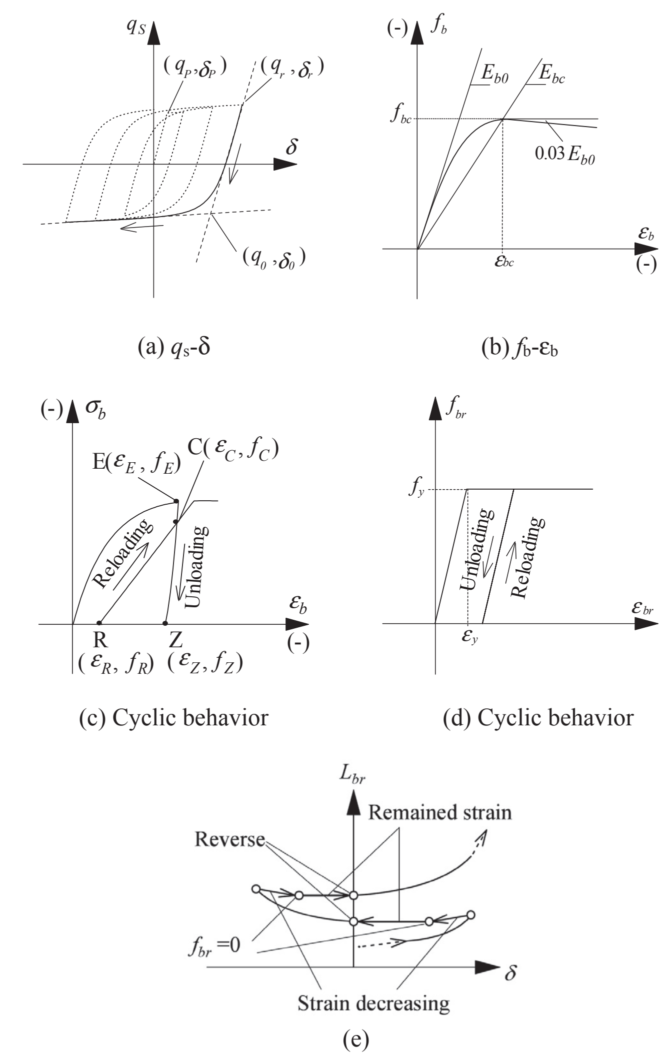

Fig. 10. Mechanical behavior of each components.

strain $\Delta\varepsilon_{br}$. The shear component force q_T^s can be obtained as follows:

$$q_T^s = q_T \cdot sin\theta = f_{br}\frac{\pi\phi^2}{4}\cdot sin\theta \tag{14}$$

4.5. Mechanical behavior of the three components

Fig. 10 shows the respective mechanical behaviors of the three components of shear force, as was calculated according to Eq. (3). In this section, the details of these mechanical behaviors are explained.

(1) *Bending Resistance of Plastic Hinge*

In this model, the bending resistance behavior of the plastic hinge is considered to be equivalent to the behavior of a reinforcing bar subjected to tensile stress. The Menegotto-Pinto model [15,16] is used here as a constitutive equation, replacing stress and strain with force q_s and displacement δ, respectively.

The shear force q_P that causes the anchor bolt to yield is obtained as follows from Eqs. (15) and (16):

$$q_P = M_P/L_h \tag{15}$$

$$M_P = \frac{\phi^3 \cdot f_y}{6} \tag{16}$$

where M_P is the plastic moment of the anchor bolt.

Here, δ_P, that is the displacement when $q_s = q_P$, is set to 0.75 mm.

(2) *Supporting Stress of Concrete*

Since the supporting stress is related to the local compressive stress in the concrete, the previous constitutive laws of compressive stresses can be applied to the supporting stress up to the level of the maximum stress [17].

$$f_b = \frac{E_{b0}\cdot\varepsilon_b}{1+\left(\frac{E_{b0}}{E_{bc}}-2\right)\left(\frac{\varepsilon_b}{\varepsilon_{bc}}\right)+\left(\frac{\varepsilon_b}{\varepsilon_{bc}}\right)^2} \tag{17}$$

Additionally, the maximum supporting stress exceeds the maximum compressive stress f_c. Fisher et al. proposed the design shear strength formula for stud bolts on the basis of the root of $f_c \times E_c$ [18]. Based on this formula, in this model, the following equation was used to obtain the maximum supporting stress f_{bc} by using the fourth root of f_c:

$$f_{bc} = 20\sqrt[4]{f_c} \tag{18}$$

After the maximum stress, the stress is slowly reducing because the concrete subjected to supporting stress is restrained. In this model, stress softening is considered, with an experimentally determined modulus that is 1% of the Young's modulus.

Fig. 10(c) shows the behavior during unloading and reloading. An unloading curve is expressed as a parabolic function through Point Z [19] in Fig. 10(c). ε_Z is the strain at Point Z, which is obtained by subtracting 0.5% of ε_{bc} from ε_E.

The reloading curve is expressed as a linear function through Points R and C. ε_R is the strain at Point R, and f_C is the stress at Point C. These strain [19] and stress values can be respectively determined as follows:

$$\varepsilon_R = \left[0.145\left(\frac{\varepsilon_E}{\varepsilon_{bc}}\right)^2 + 0.127\left(\frac{\varepsilon_E}{\varepsilon_{bc}}\right)\right]\varepsilon_{bc} \tag{19}$$

$$\varepsilon_R = \left[\frac{\varepsilon_E}{\varepsilon_{bc}} - 2.828\right]\varepsilon_{bc} \text{for} \varepsilon_E \geq 4.0\ |\varepsilon_{bc}| \tag{20}$$

$$f_C = \frac{5}{6}f_E \tag{21}$$

ε_{bc} is the strain at the peak point. Eq. (21) is applied to this model to simply reproduce the reloading path obtained in previous test results under cyclic compressive loading [20].

(3) *Tensile Stress of Anchor bolt by catenary action*

The resulting behavior of a bilinear anchor bolt model under a tensile stress is shown in Fig. 10(d). Additionally, the behavior of L_{br} subjected to cyclic loading is illustrated in Fig. 10(e). During unloading, the strain of the anchor bolt was reduced until $f_{br} = 0$. Furthermore, after the slip was reversed, the strain was found to increase again as described by Eqs. (12) and (13).

5. Adaptability of proposed model to experimental results

Fig. 11(a)–(m) shows the comparison of the results of shear load–-slip relations ($Q - \delta$ curves) obtained through experimentation and analysis.

Under the condition of actual loading, the anchor-bolt deformation occurs on the grouting mortal side. This fact must be considered. In this study, the anchor-bolt deformation was modeled as deformation of a rigid body, because the grouting mortal strength at the joint is considerably higher than that of the concrete on the exiting side.

According to Fig. 11, a larger anchor-bolt diameter results in a larger shear force Q. Additionally, increasing the tensile stress ratio r_N causes the shear force Q to decrease.

The results of specimens D13-T000-20 (Fig. 11(a)) and D16-T000-

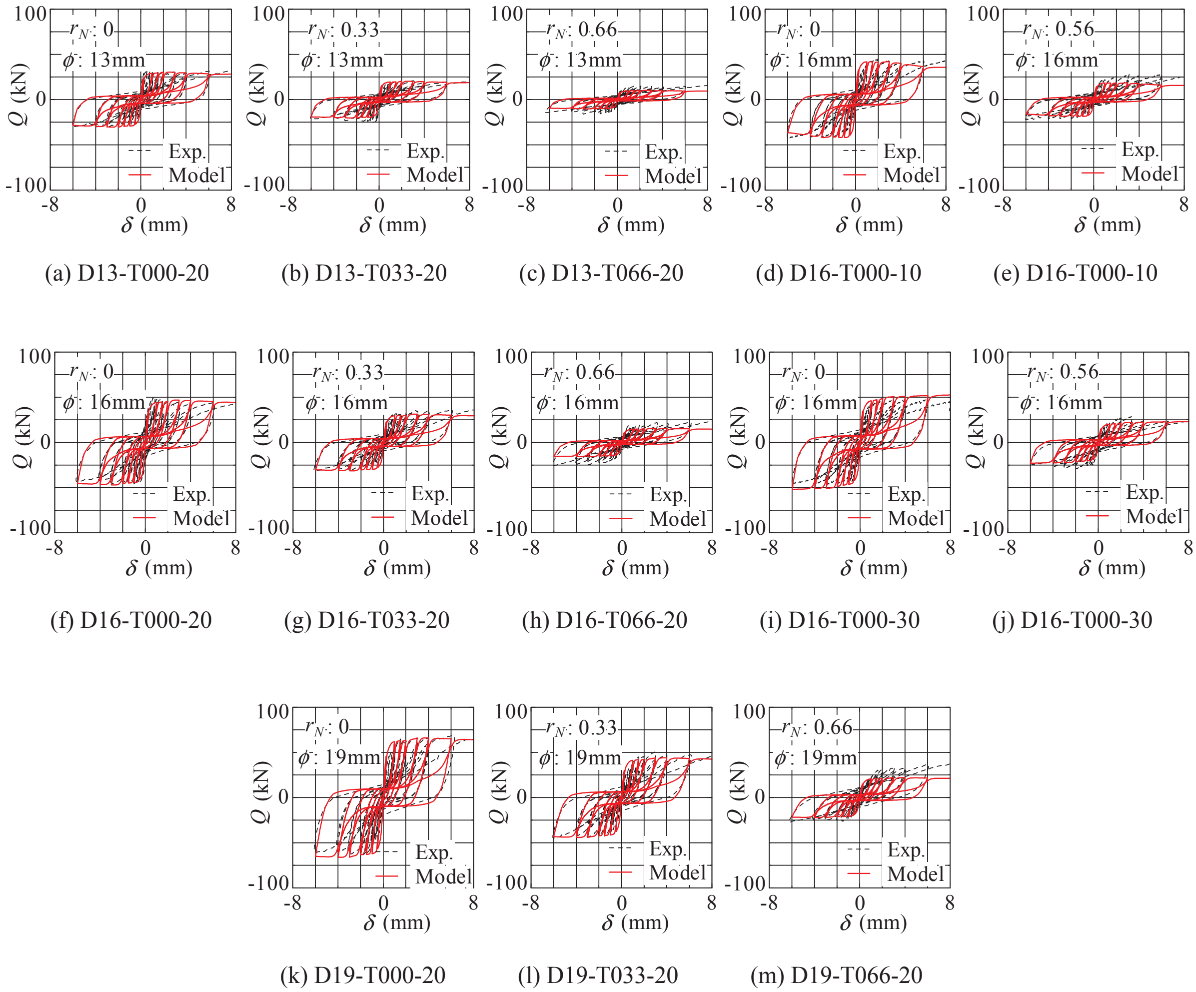

(a) D13-T000-20 (b) D13-T033-20 (c) D13-T066-20 (d) D16-T000-10 (e) D16-T000-10

(f) D16-T000-20 (g) D16-T033-20 (h) D16-T066-20 (i) D16-T000-30 (j) D16-T000-30

(k) D19-T000-20 (l) D19-T033-20 (m) D19-T066-20

Fig. 11. Shear force – slip curves.

20 (Fig. 11(f)) demonstrate that the proposed model estimates a maximum force that is slightly less than that obtained during testing. However, beyond $\delta = 1$ mm, the behaviors are predicted reasonably well. In contrast to these two specimens, the analytical stiffness of the model was found to be higher than that observed in the test results for D19-T000-20. Nevertheless, the test behavior observed beyond $\delta = 1$ mm for D19-T000-20 was appropriately evaluated by the model.

The test results of the specimens subjected to a tensile force, as illustrated in Fig. 11(b, c, e, g, h, j, l, and m) were also observed. For the specimens with $r_N = 0.33$, the test and analytical results were found to be in agreement. However, the analytical results are moderately lower than the corresponding test results for the specimens with $r_N = 0.66$. This tendency is especially apparent for D19-T066-20, as it is clearly depicted in the positive loading shown in Fig. 11(m). In this model, the phenomenon that the shear force is reduced in response to increasing tensile force is described in Eq. (4). However, although this model is useful and simple, it is not stringent. The accuracy of the model can be improved by increasing the amount of strain applied to the anchor bolt and decreasing the supporting stress of concrete under a combined force.

As was mentioned above, because the proposed model can accurately evaluate the overall mechanical behavior of post-installed anchors during unloading and reloading, it is expected to be useful in various fields of engineering, such as in the field of seismic design and analysis.

6. Conclusions

Shear loading tests were conducted in this study on concrete specimens subjected to cyclic shear force and constant tensile force. Additionally, a mechanical model was proposed for a post-installed anchor used in seismic retrofitting. In this model, the shear force is equal to the sum of the bending resistant force q_S, the supporting stress of concrete q_B, and the shear component of the tensile stress q_T^s. The findings of this study are summarized as follows:

(1) With increasing tensile force, the shear force decreases and the joint separation increases.
(2) Setting $\alpha = 0.75$–1.5 (Eq. (1)) yielded an estimation of the relationship between T/T_a and Q/Q_a that is in agreement with the testing results.
(3) By setting $\alpha = 1$ in Eq. (4), the proposed model can predict test results reasonably well.
(4) This model proposed the respective mechanical behaviors of q_S, q_B, and q_T^s under cyclic loading. Moreover, the proposed model reasonably estimates the cyclic behavior of post-installed anchors.
(5) The proposed model is useful for evaluating the shear force–slip relations of post-installed anchors subjected to a combined force.

Future work will focus on improving the model by considering the stress–slip behavior of bond adhesives, and the separation of joints. In addition, it is thought that the reinforcement ratio and the vertical loading in a structure affect the dowel action. The author will also investigate these effects in future research.

Acknowledgment

This work was partly supported by JSPS KAKENHI Grant Number JP16K18195.

Appendix A. Supplementary material

Supplementary data to this article can be found online at https://doi.org/10.1016/j.engstruct.2019.05.086.

References

[1] Sorensen JH, Hoang LC, Olesen JF, Fischer G. Testing and modeling dowel and catenary action in rebars crossing shear joints in RC. Eng Struct 2017;145:234–45.
[2] Friberg BF. Design of dowels in transverse joints of concrete pavements. Am Soc Civ Eng 1938;64(9):1809–28.
[3] Hofbeck JA, Ibrahim IO, Mattock AH. Shear transfer in reinforced concrete. J ACI 1969;66(2):119–28.
[4] Jimenez R, White RN, Gergely P. Cyclic shear and dowel action models in R/C. J Struct Eng 1982;108(5):1106–23.
[5] Millard SG. Shear transfer across cracks in reinforced concrete due to aggregate interlock and to dowel action. Mag Concr Res 1984;36(126):9–21.
[6] Vintzeleou EN, Tassios TP. Mathematical models for dowel action under monotonic and cyclic conditions. Magaz Concr Res 1986;38(134):13–22.
[7] Vintzeleou EN, Tassios TP. Behavior of dowels under cyclic deformations. ACI Strct J 1987;84:19–30.
[8] Wang D, Wu D, He S, Zhou J, Ouyang C. Behavior of post-installed large-diameter anchors in concrete foundations. Constr Build Mater 2015;95:124–32.
[9] Moradi AR, Soltani M, Tasnimi AA. A simple constitutive model for dowel action across RC cracks. J Advanced Concr Tech 2012;10:264–77.
[10] Shaheen MA, Tsavdaridis KD, Salem E. Effect of grout properties on shear strength of column base connections: FEA and analytical approach. Eng Struct 2017;152:307–19.
[11] He XG, Kwan AKH. Modeling dowel action of reinforced bars for finite element analysis of concrete structures. Comput Struct 2001;79:595–604.
[12] Soltani M, Maekawa K. Path-dependent mechanical model for deformed reinforcing bars at RC interface under coupled cyclic shear and pullout tension. Eng Struct 2008;30:1079–91.
[13] Shirai Y, Yamada S, Sakata H, Shimada Y, Kishiki S. Experimental study on mechanical behavior of anchor bolts and surrounding concrete under combined loading. J Struct Construc Engin, AIJ 2015;80(11):1735–44. [in Japanese].
[14] Takase Y, Wada T, Ikeda T, Shinohara Y. Mechanical model of adhesive post-installed anchor subjected to cyclic shear force. Proc Fract Mech Concr Concr Struct 2013:1727–36.
[15] Menegotto M, Pinto PE. Method of analysis for cyclically loaded R.C. plane frame including changes in geometry and non-elastic behavior of elements under combined normal force and bending. P of IABSE symposium on resistance and ultimate deformability of structures acted on by well defined repeated loads 1973:15–22.
[16] He Wei WuYF, Liew KM. A fracture energy based constitutive model for the analysis of reinforced concrete structures under cyclic loading. Comput Methods Appl Mech Eng 2008;197:4745–62.
[17] Saenz LP. Discussion of equation for stress–strain curve of concrete, by Desayi P and Krishnan S. J Am Concr Inst 1983;61(7):1227–39.
[18] Ollgaard JG, Slutter RG, Fisher JW. Shear strength of stud connectors in lightweight and normal-weight concrete. AISC Eng J 1971;4:55–64.
[19] Karsan ID, Jirsa JO. Behavior of concrete under compressive loading. J Struct Eng 1969;95(12):2543–63.
[20] Sima JF, Roca P, Molins C. Cyclic constitutive model for concrete. Eng Struct 2008;30:695–706.